SWIRLING JETS ISSUED FROM FULLY DEVELOPED ROTATING PIPE FLOW - EXPERIMENTS AND NUMERICS

Luca Facciolo[†], Paolo Orlandi[‡], P. Henrik Alfredsson[†]

[†]KTH Mechanics, Royal Institute of Technology
100 44 Stockholm, Sweden

[‡]Dipartimento di Meccanica e Aeronautica,
La Sapienza, Roma, Italy

ABSTRACT

Direct Numerical Simulation (DNS) and experimental data are used to study a rotating jet flow. A non-confined swirling jet is generated by a fully developed rotating turbulent pipe flow. Previous experiments have demonstrated the presence of a counter-rotating core appearing approximatively 6 diameters downstream the pipe outlet. The mean azimuthal velocity component changes its sign in the central part of the jet starting to move in the opposite direction with respect to the rotation imposed by the rotation of the pipe. The present paper introduces new investigations intended to analyse the jet flow in the proximity of this phenomenon.

INTRODUCTION

Axially rotating turbulent pipe flow is an example where rotation strongly affects the turbulence and thereby the Reynolds stresses and mean flow properties. The present paper reports new measurements and direct numerical simulations where the initial condition of a swirling jet is a fully developed rotating pipe flow. The geometry is shown in figure 1 (x is the streamwise, θ the azimuthal and r the radial direction, and the corresponding instantaneous velocity components are $U+u$, $V+v$ and $W+w$, where capital letters denote mean values and lower case letters denote fluctuations). Two parameters describe the pipe flow namely the Reynolds number ($Re = U_b 2R/\nu$ where U_b is the bulk velocity) and the swirl number ($S = V_w/U_b$, where V_w is the pipe wall velocity).

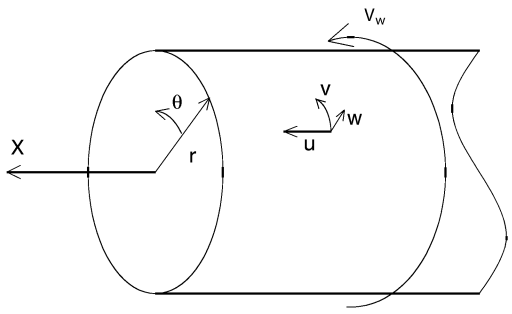

Figure 1: Coordinate system

The Reynolds averaged continuity equation in cylindrical coordinate system for a steady and axisymmetric flow is

$$\frac{\partial W}{\partial r} + \frac{W}{r} + \frac{\partial U}{\partial x} = 0 \tag{1}$$

whereas the Reynolds averaged Navier-Stokes equations become

$$U\frac{\partial U}{\partial x} + W\frac{\partial U}{\partial r} = -\frac{1}{\rho}\frac{\partial P}{\partial x} - \frac{1}{r}\frac{\partial}{\partial r}\left(r\overline{uw}\right) - \frac{\partial}{\partial x}\overline{u^2} + \frac{\nu}{r}\frac{\partial}{\partial r}\left(r\frac{\partial U}{\partial r}\right) \tag{2}$$

$$U\frac{\partial V}{\partial x} + W\frac{\partial V}{\partial r} + \frac{VW}{r} = -\frac{1}{r^2}\frac{\partial}{\partial r}\left(r^2\overline{vw}\right) - \frac{\partial}{\partial x}\overline{uv} + \frac{\nu}{r^2}\frac{\partial}{\partial r}\left[r^3\frac{\partial}{\partial r}\left(\frac{V}{r}\right)\right] \tag{3}$$

$$\frac{1}{\rho}\frac{\partial P}{\partial r} = -\frac{\partial}{\partial r}\overline{w^2} + \frac{1}{r}\left(V^2 + \overline{v^2} - \overline{w^2}\right) \tag{4}$$

Equation 3, in the case of a fully developed (i.e. no x-variation and $W \equiv 0$) axially rotating pipe flow with radius R, can be integrated to obtain the azimuthal velocity component V as

$$\frac{V(r)}{V_w} = \frac{r}{R}\left(1 - \int_r^R \frac{\overline{vw}}{\nu V_w/R}\frac{dr}{r}\right) \tag{5}$$

On the right hand side of eq. 5 the first term can be identified as a solid body rotation of the flow, whereas the second term shows the contribution from the Reynolds stress $\overline{vw}$. In a laminar flow this latter term is equal to zero and in the fully developed state the flow would be in solid body rotation. For a turbulent flow for which $\overline{vw} \neq 0$, the Reynolds stress term generates a deviation of the azimuthal velocity from that of solid body rotation. Both experiments and simulations have shown that this gives as a result that the azimuthal mean velocity distribution is close to quadratic in r, i.e.

$$\frac{V}{V_w} \approx \left(\frac{r}{R}\right)^2 \tag{6}$$

Equation 6 implies that the flow lags behind that of a hypothetical solid body rotation and that the integral of the

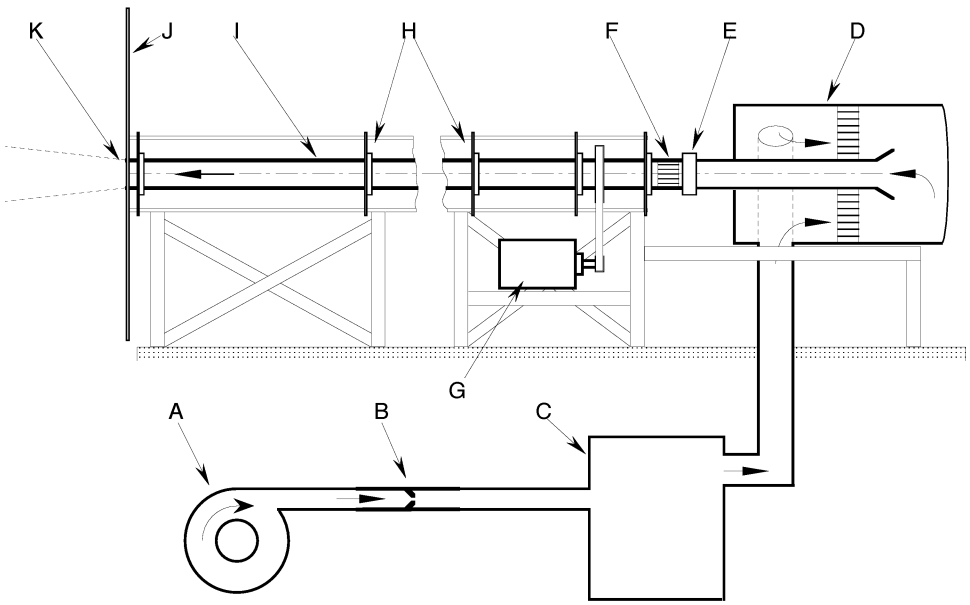

Figure 2: Schematic of the experimental setup. A) Centrifugal fan, B) Flow meter, C) Settling chamber, D) Stagnation chamber, E) Coupling-box between rotating and stationary pipe, F) Honeycomb fixed to the pipe, G) DC-motor, H) Ball bearings, I) Rotating pipe with a length of 6 m and inner diameter of 60 mm, J) Aluminum plate, K) Pipe outlet.

Reynolds stress in Eq. 5 has to be positive. This also means that the Reynolds stress $\overline{vw}$ in itself has to be positive.

EXPERIMENTAL SET-UP

The swirling jet flow is generated from a fully developed turbulent rotating pipe flow both in the DNS and in the experiment. In the experiment the pipe has a length (L) of 6 m and a diameter (D) of 60 mm (L/D=100) and is made of seamless steel with the inner surface honed. The rotation is belt driven by an electric DC motor with a feedback circuit. The flow is driven by a centrifugal fan, and before reaching the rotating pipe it passes through an axis-symmetric stagnation chamber in order to get uniform inlet conditions. At the pipe inlet, a 120 mm long honeycomb is placed inside the rotating pipe in order to bring the flow into rotation already from the inlet of the pipe. The outlet of the rotating pipe is in the centre of a flat stationary rectangular aluminium plate (80×100 cm). Figure 2 shows a schematic of the experimental set-up.

The results presented in this paper were all measured with a two component LDV-system. A single two-components laser-head has been used to measure at the same time the axial and the azimuthal velocity while, for the simultaneous measurement of the azimuthal and radial velocity components, two one-component laser-heads positioned at 90 degrees with respect to their optical axis have been used. The smoke consisting of oil droplets was introduced at the centrifugal fan. The sampling times was chosen to 20 minutes giving typically 30000 samples.

The measurements presented in this paper are made at Re ≈12800 and 24000 and swirl numbers in the range 0–0.5. It should be pointed out that for the mean flow components U and V measurements have also been made using hot wire anemometry showing similar results.

NUMERICAL CODE

The temporal swirling jet has been simulated using a finite difference DNS code developed by Verzicco & Orlandi (1996), which solves the Navier-Stokes equations in a cylindrical coordinate system. The method is based on a fractional step scheme which uses a discretization of the equations in a staggered grid that, together with the introduction of the variable $q_r = rw$, allows to overcome the singularity along the axis ($r = 0$). The code solves the equations in a rotating frame coordinate system where the Coriolis force is explicitly taken into account. The flow is treated periodically in the axial and the azimuthal direction. The grid used in the rotating pipe is $129 \times 129 \times 129$ and it is uniform in the axial and azimuthal directions and clustered at the wall in the radial direction. Results for the rotating turbulent pipe flow, using this code, have earlier been reported by Orlandi & Fatica (1997).

In order to generate a round axisymmetric swirling jet the simulation starts from the fully developed rotating pipe flow. When a steady solution is reached for the pipe flow, the wall of the pipe is removed and the domain of the simulation is increased from 1 to 4 radii. The rotating coordinate system is replaced by a fixed laboratory coordinate system and the data of the rotating pipe are adapted to the new frame of reference and all the velocity components are set initially to zero for r >1. The mesh in the domain is resized to $129 \times 193 \times 129$ using again a uniform grid in the axial and azimuthal direction

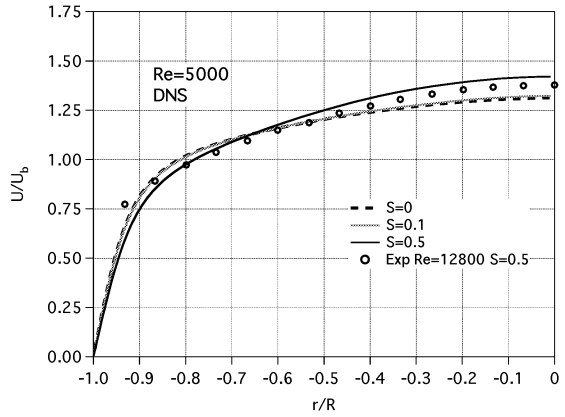

Figure 3: Streamwise velocity of the rotating pipe flow.

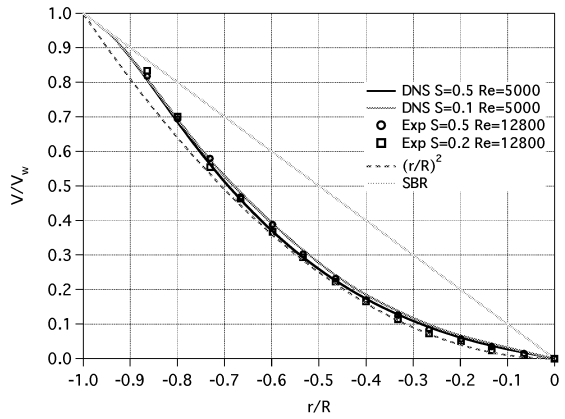

Figure 4: Azimuthal velocity of the rotating pipe flow.

and a clustered region around $r = R$ in the radial direction in order to better resolve the developing shear layer. The no-slip boundary condition at the pipe wall are replaced with free-slip conditions: in this way the flow coming from the pipe is let free to expand. Due to the periodicity in the axial and in the azimuthal direction required by the code, considering the continuity equation, it is clear that the mean radial velocity component has to be zero everywhere which means the flow can expand only by diffusion (turbulent and viscous).

The numerical simulations presented in this paper are for Re=5000 and 10000, and swirl numbers of 0, 0.1 and 0.5.

RESULTS

Pipe flow results

Figures 3 and 4 show the streamwise and azimuthal velocity distributions for the fully developed pipe flow.[1] The LDV measurements were taken just outside the pipe exit and both

[1]Note that in the figures we present data also for negative r, however for the experiments negative r just corresponds to $\theta = \pi$. All DNS data are averaged over all θ (and x) and the choice of r larger or smaller than zero is arbitrary

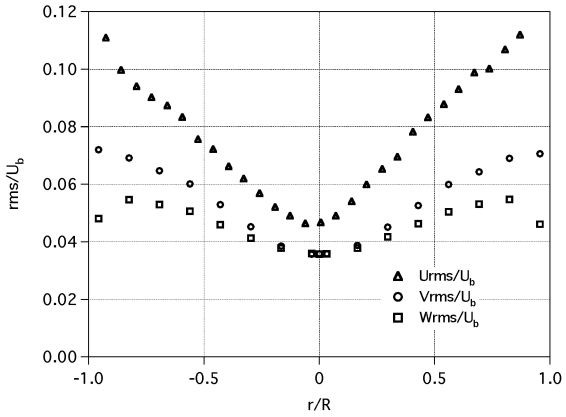

Figure 5: Turbulence intensity of rotating pipe flow measured at the outlet of the pipe. Experiment: Re=24000, S=0.5.

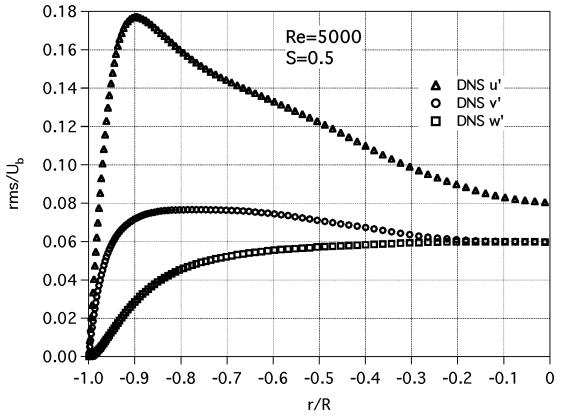

Figure 6: Turbulence intensity of rotating pipe flow. DNS: Re=5000, S=0.5.

components are measured simultaneously. The Reynolds number in the experiment is 12800 and in the simulation 5000. For the streamwise velocity the numerical simulation shows that the profile becomes less full with increasing swirl, although the effect for S=0.1 is quite small as compared to S=0. Also plotted are the experimental data for S=0.5 which are fairly close to the simulation at the same swirl number.

The azimuthal velocity distribution on the other hand show a similar distribution for all swirl numbers (simulation data for S=0.1 and 0.5, experimental data for S=0.2 and 0.5). As can be seen the two swirl numbers in the numerical simulation give almost identical profiles and the DNS-data are also in good agreement with the LDV-measurements. Close to the pipe wall ($r/R = -1$) the velocity deviates from the quadratic distribution and goes towards the solid body rotation.

Figures 5 and 6 show the turbulence intensities of all the three velocity components from the experiment and the DNS, respectively. A higher Reynolds number as the one used in the experiment shows lower values of the turbulence intensity and the relative maxima are closer to the pipe wall as would be expected. Both experiment and simulation confirm that the axial component has the higher turbulence intensity and the radial component the lower one.

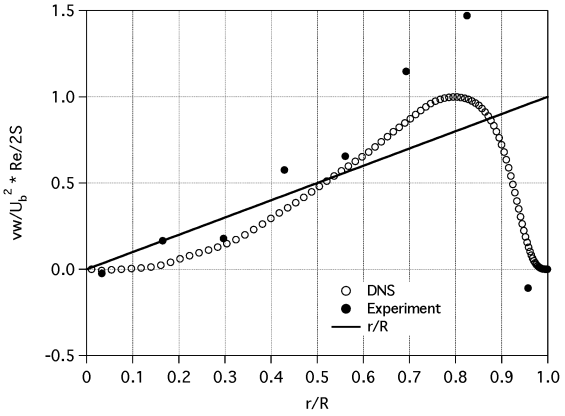

Figure 7: Normalised Reynolds stress $\overline{vw}$ at S=0.5. Experiment: Re=24000, DNS: Re=5000

Considering equation 6 it is possible to derive that, in the hypothetical case of a perfect quadratic behaviour of the azimuthal velocity, the Reynolds stress $\overline{vw}$ has to be linear in r. This linear behaviour is represented by the straight line in figure 7. The DNS data, and the experimental data are also plotted in the same figure and confirm the validity of the scaling with $Re/2S$. Furthermore, from equation 6 together with figure 4, indicates that the Reynolds stress $\overline{vw}$ is positive for all r since the azimuthal velocity is always lagging behind the solid body rotation. The experimental data point close to r/R=1 shows a negative value and that is possible to explain by the fact that the data have been collected at the outlet of the rotating pipe so the initial shear layer of the jet and a non zero mean radial component. Also inappropriate seeding in the intermittent region could affect the measurement at this position.

Jet flow results

Figure 8 shows the decay of the streamwise velocity on the centreline for both experiments and the simulation for $S = 0$ and 0.5. The time in the simulation has here been transformed to a distance using the bulk velocity and this seems to give a good agreement for the non-swirling jet. First of all it can be seen that the centreline velocity of the swirling jet decreases much faster than for the non-swirling jet both in the experiments and the simulation. This is due to the fact that the spreading of the jet increases with rotation.For the swirling jet the agreement is somewhat worse but still acceptable with regard to the simplification made in the model.

Figures 9 and 10 display the development of the axial and the azimuthal mean velocity in the jet. The measurements (Re=24000, S=0.5) reveal the spreading of the jet and the decay of the velocities. In particular, the behaviour of the azimuthal velocity at x/D=6 in the core of the jet has attracted our attention.

Figure 11 and 12 show the normalised mean axial velocity component U/U_b and the azimuthal velocity component V/V_w measured at x/D=5, 6, 7 for Re=24000 and S=0.5 to highlight the region where the change in rotation direction is observed. The two-velocity component LDV system simultaneously measured the axial and the azimuthal velocity profiles. The attention was focused to the central region of the jet, i.e.

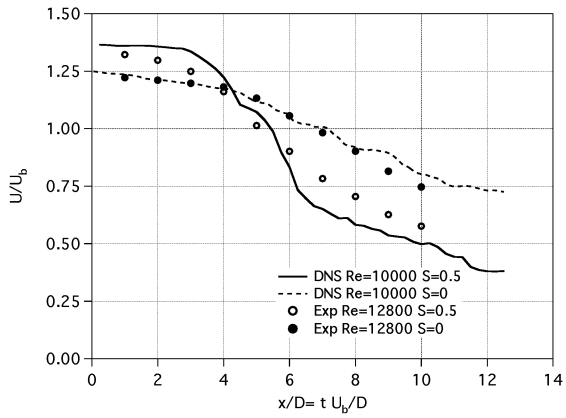

Figure 8: The decay of the centreline velocity for non-rotating (S=0) and rotating (S=0.5) jet flow. Comparison between experimental data and DNS.

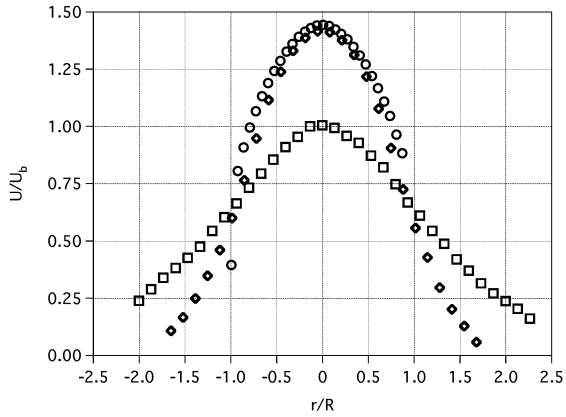

Figure 9: Axial velocity measured at x/D=0, 2 and 6. Re=24000, S=0.5.

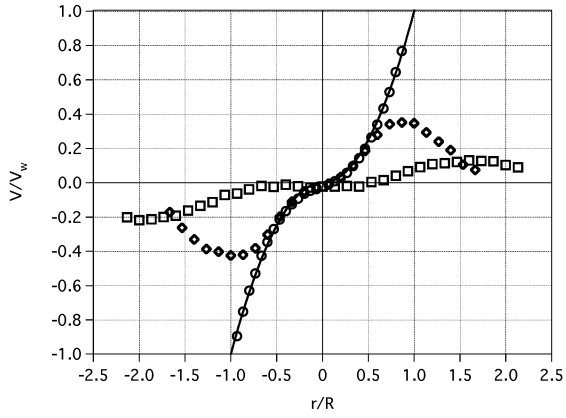

Figure 10: Azimuthal velocity measured at x/D=0, 2 and 6. Re=24000, S=0.5.

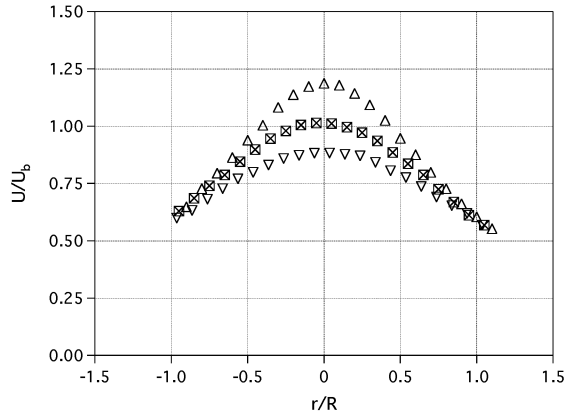

Figure 11: Axial velocity measured at x/D=5, 6 and 7. Re=24000, S=0.5.

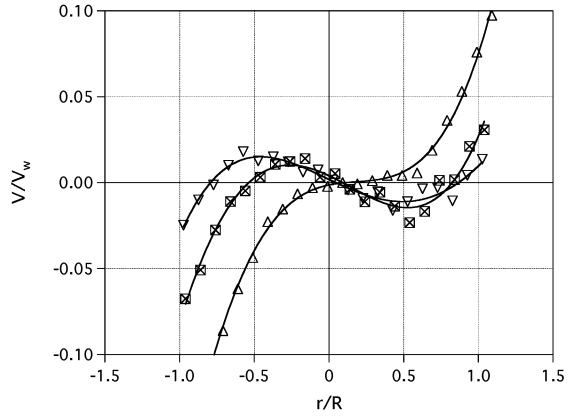

Figure 12: Azimuthal velocity measured at x/D=5, 6 and 7. Re=24000, S=0.5.

$|r/R|$ <1. The axial velocity distribution was used to centre the jet, i.e. to find $r = 0$ and the resulting profiles can be seen in Figure 11.

The three profiles in figure 12 show the downstream evolution of V/V_w. The solid lines in the figure are polynomial fittings to the experimental data drawn for visual aid. At x/D=5, the velocity profile is still monotonic, although it seems to be somewhat off-axis with respect to the mean axial component. Note that the same shifts in r as were used for the streamwise velocity are also used here. In the rotating pipe V/V_w=0.25 at r/R=0.5 which shows that already here there is a large reduction of the azimuthal velocity component. Proceeding downstream to x/D=6 and 7, the profiles show a change in sign of the azimuthal velocity.

Figure 13 shows the azimuthal velocity distribution obtained from the numerical simulation at 8 different times. Again using U_b to transform from time to distance the times correspond to x/D=0.25, 1.25, 2.5, 3.75, 5, 7.5, 10 and 12.5. As can be seen the back flow seems to start at an x/D slightly larger than 5, which are in good agreement with the experimental results shown in figure 12. At the furthest downstream position the size of the counter-rotating region corresponds to the diameter of the pipe and the maximum of the negative az-

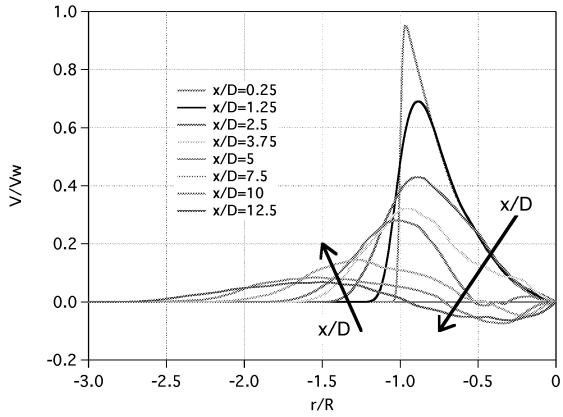

Figure 13: Azimuthal velocity obtained from the numerical simulation at 8 different times, corresponding to x/D=0.25, 1.25, 2.5, 3.75, 5, 7.5, 10 and 12.5. Re=5000 and S=0.5.

imuthal velocity is of the order of $0.07V_w$. Although this value is larger than what was observed in the experiments the qualitative agreement between the experiments and the simulation is good.

The turbulence fluctuations for the azimuthal and the radial component are plotted in figure 14 and 15. The fluctuations in the azimuthal velocity is decreasing in the downstream direction (with the exception of the centreline). On the other hand, the radial component exhibit a different trend since it increases moving from x/D=5 to x/D=6 and then, moving at x/D=7, it decreases to a lower level becoming almost constant along the radius. The azimuthal and the radial turbulence fluctuation reach almost the same magnitude for x/D=7.

The azimuthal-radial Reynolds stress $\overline{vw}$ for the investigated downstream positions is plotted in figure 16. The Reynolds stress $\overline{vw}$ should be zero at the centreline due to symmetry. For visual aid linear fits are made to the data in the region $0.25 < |r/R| < 1$ which are in fairly good agreement on both sides. The same scaling used for the pipe flow has been applied also here and it is clear that the magnitude of the Reynolds stress has increased with more than an order of magnitude from its value at the end of the pipe. For all the three downstream positions the azimuthal-radial Reynolds stress is linear with the radius, at least in the outer part. The slope of the lines decreases as the flow moves downstream showing the decay of $\overline{vw}$ in this region. It is not possible to obtain $\overline{vw}$ from the simulation since it is developing in time which does not allow enough data at each time step to determine this quantity with sufficient accuracy.

CONCLUSIONS

First we conclude that the pipe simulation can accurately reproduce the experimental results from the pipe and give good initial conditions for the simulation of the jet.

The counter rotation of the central part of the jet is an unexpected feature of the flow, but has been observed earlier in experiments. The present simulations confirm the previous experimental results. The new measurements show that the Reynolds stress $\overline{vw}$ becomes very large in the jet and it is clear that it has a significant influence on the development of the rotation of the central part of the jet.

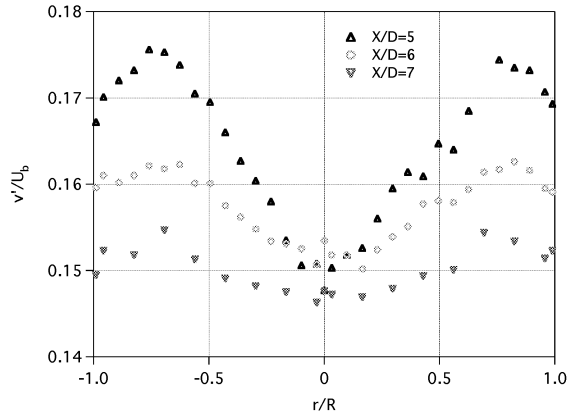

Figure 14: Azimuthal turbulence intensity measured at x/D=5, 6 and 7. Re=24000 and S=0.5.

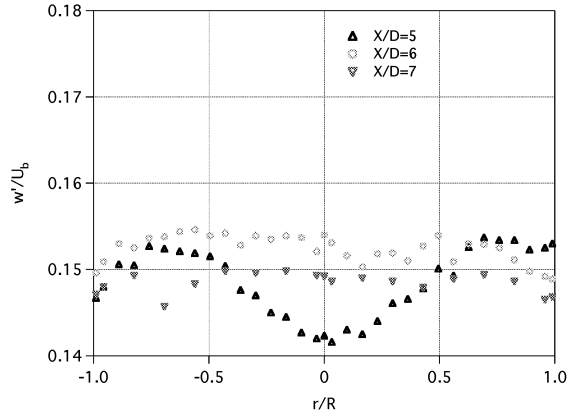

Figure 15: Radial turbulence intensity measured at x/D=5, 6 and 7. Re=24000 and S=0.5.

We offer the following physical interpretation for this behaviour: in rotating turbulent pipe flow the balance between the viscous stress and the Reynolds shear stress $\overline{vw}$ gives a near quadratic distribution of the azimuthal component, i.e. the flow is lagging behind a hypothetical solid body rotation. When the flow leaves the pipe and the forcing at r/R=1 is relaxed, the rotation of the outer part of the jet slows down, whereas at first the central part is not affected. However since the forcing is relaxed, there is no longer any force to balance $\overline{vw}$, which as a result will force the azimuthal component in the opposite direction as compared with the pipe rotation direction. Around x/D=6 the cumulative effect of this forcing is sufficient to make the core of the jet counter-rotating.

We can also see directly from eq. 3 that changes of V in the downstream direction (the first term of the LHS of eq. 3, which can be estimated to be much larger than the other two terms on the LHS) are due to the terms on the RHS, where the first term is estimated to be the most important. As can be seen it is negative and constant in the region where $\overline{vw}$ is proportional to r, which would then give $\partial V/\partial x < 0$. A further analysis of all the terms are however necessary although it is clear that the development of $\overline{vw}$ from the pipe outlet and onwards is a crucial component in obtaining the counter-

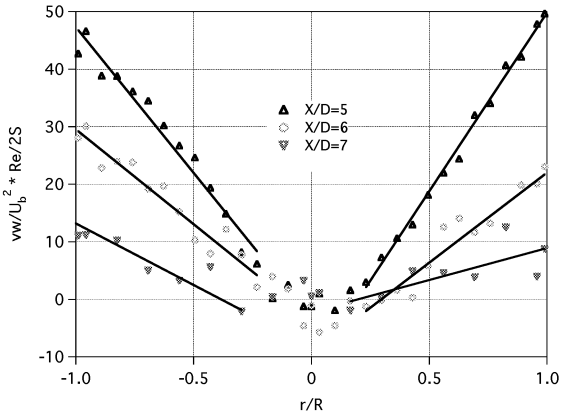

Figure 16: Azimuthal-radial Reynolds stress ($\overline{vw}$) at x/D=5, 6 and 7. Re=24000 and S=0.5.

rotating core. Future LDV measurements will be carried out to map out the development closer to the pipe outlet and also PIV-measurements are planned. It is clear that this case will be an excellent test case for advanced turbulence models which are designed to model rotation effects accurately.

ACKNOWLEDGEMENTS

This work is financially supported by the Swedish Energy Agency (STEM). We acknowledge gratefully the help with the experiments and fruitful discussions by Nils Tillmark and Alessandro Talamelli.

REFERENCES

Facciolo, L. & Alfredsson, P. H., 2004, "The counter-rotating core of a swirling turbulent jet issued from a rotating pipe flow", *Phys. Fluids*, vol. 16, pp. L71-L73.

Imao, S., Itoh, M & Harada, T., 1996, "Turbulent characteristics of the flow in an axially rotating pipe", *Int. J. Heath Fluid Flow.*, vol. 17, pp. 444-451.

Orlandi, P. & Fatica, M. 1997 "Direct simulations of turbulent flow in a pipe rotating about its axis", *J. Fluid Mech.*, vol. 343, pp. 43–72.

Verzicco, R. & Orlandi, P., 1996, "A finite-difference scheme for the three-dimensional incompressible flow in cylindrical coordinates", *J. Comp. Phys.*, vol. 123, pp. 402-414.